Biological Response to the Dynamic Spectral-Polarized Underwater Light Field

Molly E. Cummings
Section of Integrative Biology C0930
University of Texas
Austin, TX 78712
phone: (512) 471-5162   fax: (512) 471-3878   email: mcummings@mail.utexas.edu

Co-PI: Samir Ahmed (City College of New York)
Co-PI: Heidi Dierssen (University of Connecticut)
Co-PI: Alexander Gilerson (City College of New York)
Co-PI: William F. Gilly (Stanford University)
Co-PI: George Kattawar (Texas A & M University)
Co-PI: Brad Seibel (University of Rhode Island)
Co-PI: James Sullivan (University of Rhode Island)

LONG-TERM GOALS

Camouflage in marine environments requires matching all of the background optical properties: spectral, intensity and polarization components─ all of which can change dynamically in space and time. Our research investigates the biological challenge of camouflage in the near-shore littoral zone and near-surface marine environments in two distinct water types found in coastal environments around the globe (oligotrophic and eutrophic). We aim to characterize the dynamic light field along with the behavioral and cellular response of camouflaging animals in these environments. Our long-term goal is to identify the biological pathways for concealment against the underwater spectral-polarized light field enabling us to identify design principles for future naval camouflage.

OBJECTIVES

(1) Measure and model the underwater spectral-polarized light field in oligotrophic and eutrophic systems

(2) Quantify the biological response in fish and cephalopods to these dynamic underwater optical environments

(3) Identify the internal controls and structural mechanisms that coordinate the camouflage response in fish and cephalopods

1. REPORT DATE **2010**	2. REPORT TYPE	3. DATES COVERED **00-00-2010 to 00-00-2010**
4. TITLE AND SUBTITLE **Biological Response to the Dynamic Spectral-Polarized Underwater Light Field**		5a. CONTRACT NUMBER
		5b. GRANT NUMBER
		5c. PROGRAM ELEMENT NUMBER
6. AUTHOR(S)		5d. PROJECT NUMBER
		5e. TASK NUMBER
		5f. WORK UNIT NUMBER
7. PERFORMING ORGANIZATION NAME(S) AND ADDRESS(ES) **University of Texas,Section of Integrative Biology C0930,Austin,TX,78712**		8. PERFORMING ORGANIZATION REPORT NUMBER
9. SPONSORING/MONITORING AGENCY NAME(S) AND ADDRESS(ES)		10. SPONSOR/MONITOR'S ACRONYM(S)
		11. SPONSOR/MONITOR'S REPORT NUMBER(S)
12. DISTRIBUTION/AVAILABILITY STATEMENT **Approved for public release; distribution unlimited**		
13. SUPPLEMENTARY NOTES		
14. ABSTRACT		
15. SUBJECT TERMS		

16. SECURITY CLASSIFICATION OF:			17. LIMITATION OF ABSTRACT	18. NUMBER OF PAGES	19a. NAME OF RESPONSIBLE PERSON
a. REPORT **unclassified**	b. ABSTRACT **unclassified**	c. THIS PAGE **unclassified**	**Same as Report (SAR)**	**24**	

APPROACH

Our first aim is to **measure and model the underwater spectral-polarized light field** in distinct water types (oligotrophic and eutrophic). The spectral-polarized light field will be measured by the simultaneous deployment of a comprehensive optical suite including underwater video-polarimetry (Cummings), inherent optical properties, (LISST by Dierssen), hyper-spectral mulit-angular Stokes vector spectroradiometry (Gilerson and Ahmed), and the volume scattering function measures (MASCOT by Sullivan). These measurements will be used to refine development of, and make comparisons to, theoretical expectations from a fully 3-D radiative transfer model that solves for each of the polarization elements of the Mueller matrix transformation of the Stokes vector by (Kattawar), as well as to set boundary conditions for laboratory experiments.

The first modeling objective of this proposal is to calculate the complete Mueller matrix/Stokes vector for any set of oceanic and atmospheric conditions for any region of the ocean. We will then use this modeling approach (*i*) to predict the 3-D light field; (*ii*) to calculate experimental conditions to measure biological responses; and (*iii*) to investigate the nature of the light field as it interacts with cells within the skin. Our approach is to modify the 1D Monte Carlo codes of Kattawar (1) and the RayXP code of Zege (2) to develop a 3-D Monte Carlo model with full Mueller matrix treatment.

Our second objective is to **quantify the biological response to these dynamic optical environments** by field observations and laboratory measurements of vertebrate and invertebrate animals. For this second objective, we will quantify background matching of animals in their native near-shore and near-surface environments using a diver-operated video polarimeter (Cummings), and also in a laboratory setting that allows us to recreate and manipulate optical measurements recorded in the field (Cummings, Dierssen, Sullivan, Ahmed, Gilerson, Seibel, Kattawar). Specialized experimental tanks that allow for manipulating isolated components of the incident light field (e.g. altering the e-vector orientation without changes in intensity) will be employed to test the animals range of response. Animal response will be measured using the underwater video polarimeter, hyperspectral imager, and stokes vector radiometer.

Our third objective is to **identify the internal control and structural mechanisms that coordinate the camouflage response**. Here we plan to provide novel advances in our understanding of camouflage control by (a) examining both iridophore and chromatophore control processes for specific background radiance matching (spectrum and polarization plane) in live, awake animals during the adaptation process (Cummings), (b) thoroughly examining local or peripheral control features (Seibel, Gilly), and (c) developing a novel 3D Monte Carlo model to describe how the spectral-polarized light field interacts with cells within the skin (Kattawar).

Using both field-studied and model organisms, we will employ three approaches: (*i*) confocal imagery of live-awake light adapted fish using autofluorescence to identify cell types (Cummings), (*ii*) calcium-imaging optical technique to track the neural control pathway in coordinating a camouflage response in awake animals as well as prepared tissue (Seibel; Gilly; Cummings), (*iii*) Green-Flourescent Protein (GFP)-labeling of specific cell types (iridophores, melanophore and xanthophore) in zebrafish mutant lines to image the real-time response of these cells orchestrating a camouflage response (Cummings). Through these approaches we will characterize the internal control features regulating camouflage in both fish and cephalopods. We will also develop a novel use of Mueller matrix modeling to calculate the interaction of the light field within animal tissues (Kattawar).

WORK COMPLETED

a) Completed construction of experimental tanks for manipulating optical conditions and measuring fish responses (Fig 1) (Cummings, Gilerson, Ahmed).

b) Completed construction of the Underwater VideoPolarimeter (Cummings).

c) Preliminary field work in January 2010 in Port Aransas. We investigated various experimental tank setups to explore fish response to different optical environments and developed 3 channel miniature fiber optic polarization probe to make measurements. (Cummings, Gilerson, Ahmed).

d) Presented at the ONR Optics review in February 2010 (Cummings)

e) Convened for a field planning meeting at the Ocean Sciences Meeting in Portland in February (Dierssen, Seibel, Kattawar, Gilly, Sullivan, Ahmed, Gilerson, and collaborator Twardowski).

f) Measurements of Texas coastal fish skin preparations with the HyperSpectral Imager mounted on a stereomicroscope in Norway in April (Dierssen).

g) Camouflage acclimation studies with Flounder completed in the lab in April (Cummings).

h) Additional radiance sensor was installed on the CCNY polarization probe to measure circular polarized component of the light field together with linear polarization components (Gilerson).

i) First field season in Port Aransas, TX. Complete suite of optical measurements were collected in distinct habitats (seagrass (< 1.5 m, and 20 miles offshore 1- 5m depth) on multiple days in June (Dierssen, Gilerson, Sullivan, Cummings). Lab experiments were also conducted measuring polarization responses of offshore and inshore fish to specific optical conditions (Cummings); and preliminary measurements of polarized reflectance from seagrass (Dierssen).

j) Recorded *in situ* chromatic behaviors of Humboldt squid (*Dosidicus gigas*) in the Gulf of California (Table 1) using a Crittercam package (National Geographic Remote Imaging Unit). Deployments were during daytime, and no artificial lighting was employed (Gilly).

k) Completed video analysis from remotely operated vehicle of the squid, *Dosidicus gigas*, to construct an ethogram of body patterns and chromatophore displays; and initiated development of experimental tank setups for behavioral assays of squid response (Seibel).

l) Initiated development of confocal microscopy techniques to identify cell processes on live awake fish (flounder) in collaboration with Dr. Stuart Thompson of Stanford University (Cummings), and squid with Donal O'Malley at Northeastern University (Seibel).

m) Completed development, rigorous testing, and implementation of an automatic switching polarizer module (POLMOD) for use with the MASCOT VSF device (Fig 2) (Sullivan).

n) Using the Discrete Dipole Approximation(DDA) method, we have computed the optical properties, which include the phase function and scattering cross section, for a large collection

of iridosomes with various sizes, layer numbers, and for different incident wavelengths. (Kattawar)

o) A 3D Vector Monte Carlo code is developed for the calulation of skin coloration and patterns aribitrary using any cell configuration along with their optical properties. The phase function of iridosomes are calculated for random orientation. Using these optical parameters, we can use our 3-D polarized radiative transfer model to couple the light fields to predict the reflected light field off bulk skin tissue. Moreover, an extension of the Monte Carlo code for the cells with fixed orientation are developed. We have created a database of Mueller Matrices, which also include the phase function and the backward scattering efficiency, for various sizes, number of layers, and orientations of the iridosomes. (Kattawar).

RESULTS

(i)   (Dierssen) Hyperspectral Images from skin preparations of different species of fish found in coastal waters of Texas showed that spectral reflectance from chromatophores differed according to spatial location on the fish (Figs 3-4).

(ii)   (Ahmed, Gilerson) Measurements in the fish experimental tanks exhibited natural ranges of degree of linear polarization (DoLP,Fig 5) without affecting the total intensity level (Fig 6).

(iii)   (Gilerson) Stokes vector radiometric polarization measurements of light in eutrophic seagrass exhibited very unusual distributions of the degree of linear polarization (DOLP) and circular polarization (DOCP) in shallow waters. Examples of these distributions in the main plane are shown in Fig. 7. Fig. 8 shows the angular dependence of both the DOLP and DOCP in open ocean waters, in this situation the DOCP is identically zero (and very noisy).

(iv)   (Sullivan) Inherent Optical Property (IOP) measurements were taken at several sites around the Port Aransas coast (TX). The first of three eelgrass habitats was extremely turbid (~ 20 to 35 m^{-1} beam c). As estimates of [$chl\ a$] were ~ 4 $\mu g\ l^{-1}$, the bulk of light scattering was assumed to be due to detritus and/or re-suspended sediments. The other two eelgrass sites were more protected from wind mixing, thus total scattering was much lower (~ 5 m^{-1} beam c). The IOPs at these two sites were very similar (Fig 9), with [$chl\ a$] estimated at < 1 $\mu g\ l^{-1}$, again indicating that re-suspended materials were likely dominating scattering. Even though the variation in the magnitude of IOPs was large, the shape of the VSF phase functions were relatively consistent. This result may ease modeling efforts, and could indicate that organisms do not require specialized camouflage adaptations for different eelgrass habitats (i.e. the optical environment may be relatively consistent across different locations). The two offshore sites were blue-water conditions (Fig 10). Beam c was over two orders of magnitude lower than in the eelgrass environments, with [$chl\ a$] < 0.1 $\mu g\ l^{-1}$. Under these conditions, the IOPs of the water itself could be as significant as the resident particles to determining the nature of the light field and biological adaptations, in contrast to eelgrass habitats where the influence of particles dominates the light field. As expected, the Degree of Linear Polarization (DoLP) at each habitat types was quite different (Fig. 11). The eelgrass habitat DoLP was consistent with significant influence from organic particles, indicating that wind-mixed particle fields in these habitats are more organic in nature (e.g. detrital flocs) and not re-suspended bottom sediments.

4

(v)   (Dierssen) Benthic reflectance from the seagrass *Thalassia testudinum* canopy and from the sediment collected with the DOBBS are shown in Fig. 12.   Sediment reflectance ranged from 20-30% and seagrass reflectance followed measurements taken in other regions. Laboratory polarized reflectance measurements of seagrass indicate possible reflection of polarized light from seagrasses and *Sargassum sp*. (Fig 13).

(vi)   (Cummings) Underwater videopolarimetry measurements of the background Angle of Linear Polarization in the horizontal viewing plane of the fish varied by solar zenith angle (Figs. 14, 15). Noontime measurements collected in the seagrass stations exhibited nearly uniform DoLP in all azimuthal viewing direction (Fig 14), whereas sunset conditions produced a complex AoLP viewing environment where the major e-vector differed significantly at each orthogonal axis (Fig 15).

(vii)   (Cummings) UW videopolarimeter measurements of offshore fish (Lookdowns, *Selene vomer*) in the lab allowed the controlled evaluation of fish intensity, DoLP, AoLP, DoCP and AoCP (angle of circular or elliptical polarization) (Fig 16). Analyses of midflank measurements of 7 lookdowns revealed two different polarization reflectance strategies in high vs low DoLP illumination conditions (Fig 17-19, unpublished data). We have found species-specific responses to changes in the polarized light field. These offshore fish match the incident AoLP in high DoLP but not in low incident DoLP conditions (Fig 17). They also exhibit higher DoLP in conditions that mimic higher solar zenith angles with higher DoLP (and horizontal incident e-vectors), Fig 18 (top); yet show no differential DoLP under low incident DoLP conditions (Fig. 18, bottom). We also found that fish showed greater variation in AoLP in the most complex optical conditions (conditions that mimicked low solar elevation angles and varied AoLP conditions, eg. 45° incident; Fig 19). This variation was only found under high DoLP conditions (top Fig 19) but not low (bottom, Fig 19).

(viii) (vi)   (Gilly) Camera-bearing squid displayed vertical movements similar to those seen with pop-up satellite tags (Fig. 20; unpublished data), indicating that the animals were not unduly impaired. Squid in view displayed several stereotyped chromatophore patterns (Fig. 21). The most dramatic behavior was intense flashing of the entire body (Fig. 22), switching between the Clear and Dark patterns at ~ 3Hz in bursts of activity (Fig. 23A). In addition, a constant low-amplitude, flickering was visible on the head and arms of the camera-bearing squid at nearly all times. Flickering proceeds with a similar but not identical time course at adjacent spots (Fig. 23B). Rapid chromatophore expansions (darkening) and relaxations tend to be highly synchronized in time (often as synchronized as flashing), but the amplitude of both responses varies spatially in a seemingly random nature. Propagated waves of activity are not evident.

(ix)   (Seibel) We tested the hypothesis that squid species from highly complex environments (e.g. coastal benthic) would demonstrate higher diversity of displays and patterns than species from more uniform environments (e.g. deep and open ocean). We found that *D. gigas* has a catalog of components comparable to cephalopods from nearshore environments, with 29 chromatic, 15 postural, and 6 locomotory components. Of all observations, 68% included *countershading*, suggesting that crypsis for predator avoidance and prey capture is important.

(x)   (viii) (Kattawar) Modelling examination of cephalopod camouflage shows that changing optical thickness and size changes backward scattering efficiencies (Fig 24-26). The size effect plays an important role for the small scatterers (Fig 24). The backward scattering efficiency deviates more and more from the semi-infinite plate case (the thick blue curve) when its radius is decreasing. Enhancement of the backward scattering efficiency is obtained by letting more and more layers contribute to the constructive interference (Fig 24). The maxium backward scattering efficiency is around 410nm (Fig 25), and this peak is preserved in the multiple scattering results as shown in our Monte Carlo results (Fig 26). Moreover, there is relatively high reflection at shorter wavelengths, even when their backward scattering efficieny is low (Fig 25). This is because the scattering efficiency is high at the shorter wavelengths, and it will result in a larger optical depth at shorter wavelength. From the comparison of the layer thicknesses of 5 μm and 10 μm, increasing the optical depth will increase the difusse reflection (Fig 26). With the infinite optical depth, the reflection will approach to 1.

IMPACT/APPLICATIONS

Understanding the underlying controls of biological camouflage may be used in the future to simulate the camouflage response artificially to enhance clandestine naval operations underwater.

RELATED PROJECTS

This ONR project, benefits from the leveraging of funding by NOAA CREST in which remote sensing of coastal waters is an important component. The CCNY group also partially studies polarization characteristics of light in water through another award from ONR N00014-10-1-0368 for years 2009-2012 with the emphasis on the remote sensing applications and improvement of the underwater visibility.

This ONR project benefits from leverage funding by NSF (to Seibel; co-PI Sonke Johnsen) to study *"Midwater animal models: optical measurement of metabolic transitions in transparent biota"* from 2009-2012 that includes 4 wweeks of shiptime and 10 days of submersible time. It also benefits from leveraged funding from NSF (to Seibel and Gilly) to study *"Hypoxia and the ecology, behavior and physiology of jumbo squid, Dosidicus gigas"* from 2009-2012 including 8 weeks of shiptime.

PUBLICATIONS

A. Tonizzo, A. Ibrahim, J.Chowdhary, A. Gilerson, S. Ahmed, "Estimating particle composition from the polarized water leaving radiance," Ocean Optics, XX, Anchorage, AK, 2010 [published].

V.P.Budak, D.S. Efremenko, A. Gilerson, D.A. Klyuykov, S.V.Korkin, S.L. Oshchepkov, A. Tonizzo, S. Ahmed, "CIAO: model of polarization radiation transfer in atmosphere – ocean system," Ocean Optics, XX, Anchorage, AK, 2010 [published].

A. Tonizzo, T. Harmel, A. Ibrahim, S. Hlaing, I. Ioannou, A. Gilerson, J. Chowdhary, B. Gross, F. Moshary and S. Ahmed, "Sensitivity of the above water polarized reflectance to the water composition," Proc. of SPIE 7825, 2010 [published].

A. Tonizzo, A. Ibrahim, J. Zhou, A. Gilerson, M. Twardowski, B. Gross, F. Moshary, and S. Ahmed, "Estimation of the polarized water leaving radiance from above water measurements," Proc. of SPIE, 7678, Ocean Sensing and Monitoring, Weilin (Will) Hou, Editor, April 2010 [published].

J. Zhou, A. Tonizzo, A. Gilerson, B. Gross, F. Moshary and S. Ahmed "Under water polarization characteristics and their impact on in water visibility," Proc. of SPIE, 7678, Ocean Sensing and Monitoring, Weilin (Will) Hou, Editor, April 2010 [published].

HONORS/AWARDS/PRIZES

Ocean Optics XX *Conference Chair* (Dierssen)

Ocean Optics XX *Plenary Speaker* (Kattawar)

Ocean Optics XIX *Best Speaker Award* (Cummings)

Table 1. Summary of Crittercam deployments on Humboldt squid. Release time is local time. Averages are means ± 1 SD. 2009 deployments were made near Santa Rosalia, BCS, Mexico from the chartered vessel Sandman (La Paz, BCS). 2010 deployment was made near Bahia Los Angeles, BC, Mexico from the UNOLS R/V New Horizon. The camera package for Squid 3 never reported via VHF radio, and we were unable to recover it.

Squid	Date (m/d/y)	Lat. (°N)	Long. (°W)	Mantle Length (cm)	Release Time	Duration (min)	Average Temp.(°C)	Average Depth (m)	Maximum Depth (m)
1	06/09/09	27.54	112.3	>80	16:04	150	21 ± 3	76 ± 20	113
2	07/09/09	27.54	112.3	>80	16:49	106	19 ± 4	116 ± 48	167
3	10/06/10	28.64	113.06	76	06:45	--	--	--	--
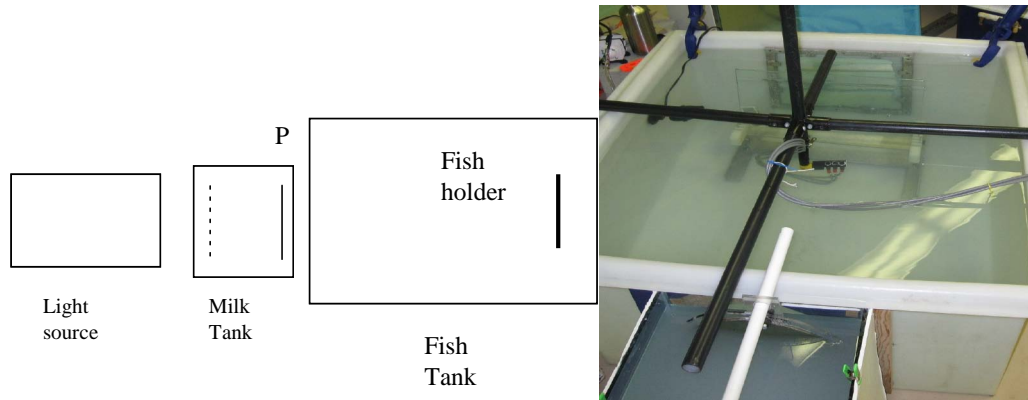
Fig. 1. Scheme of experimental setup and one of its implementations with fiber optics polarization probe, milk tank with polarizer (P) in the front or back (dashed line) and the fish holder. {This setup allowed for a uniform incident light, whose direction of polarization and degree of linear polarization (DoLP) can be varied without affecting the total intensity level. This was achieved by the installation of additional 'milk' tank(s) with controlled concentration of milk or equivalent substance (Maalox). Film polarizers on the special frames were installed on the way of the incident light in the milk tank. Parallel light from 1kW lamp which passed the milk tank was polarized to various degrees depending on the position of the polarizer with the maximum DoLP achieved when the polarizer was at the end of the tank closest to the fish tank. Direction of polarization was changed by the rotation of the polarizer in the milk tank.}

Fig2. Schematic drawing (left) of the POLMOD and the finished device integrated into the MASCOT (right). The POLMOD consists of a rotating wheel with several polarization filters and control electronics, and is installed in front of the MASCOT laser source.
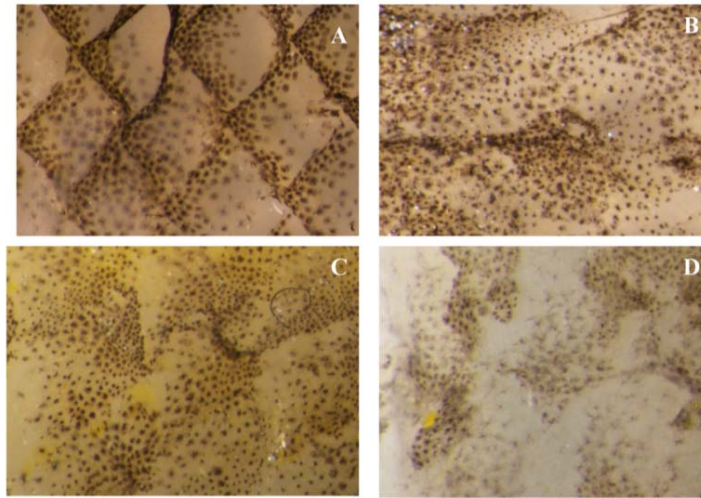
Fig 3. Skin preparations viewed under magnification different fish species that inhabit different water environments (A,B) near-surface inhabitants, and (C) seagrass (pinfish) and (D) sand (Southern flounder).   These images are reconstructed from vertical image slices to provide a spatial resolution of approximately 0.004 mm^2 per pixel or 240 pixels per mm^2, a resolution high enough to isolate different pigment cells on the skin.
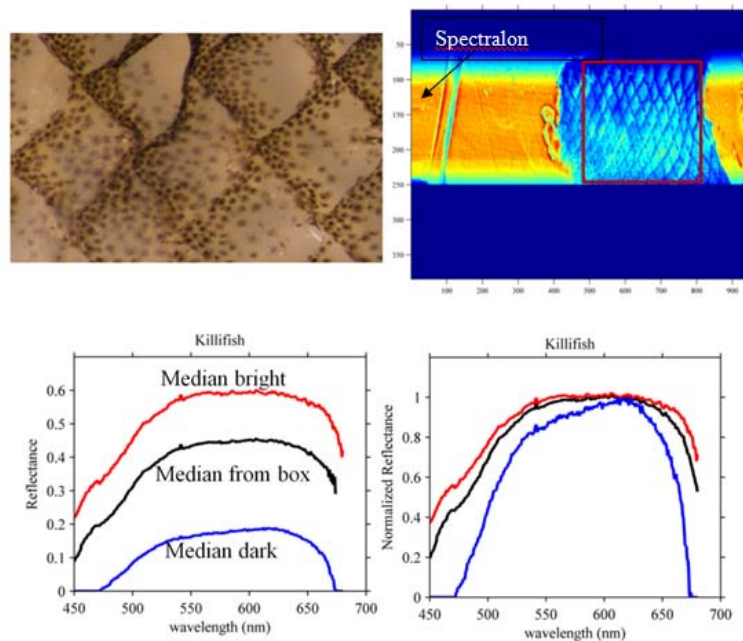
Fig 4. A) Picture of the red-brown chromatophores visible on fish skin preparations. B) Matlab image of skin preparation showing the boxed area used in the spectral analysis. C) Median reflectance spectra from the boxed region in panel B. D) Spectra normalized to reflectance at 612 nm showing the more red-brown spectra of the dark pigmented chromatophores.
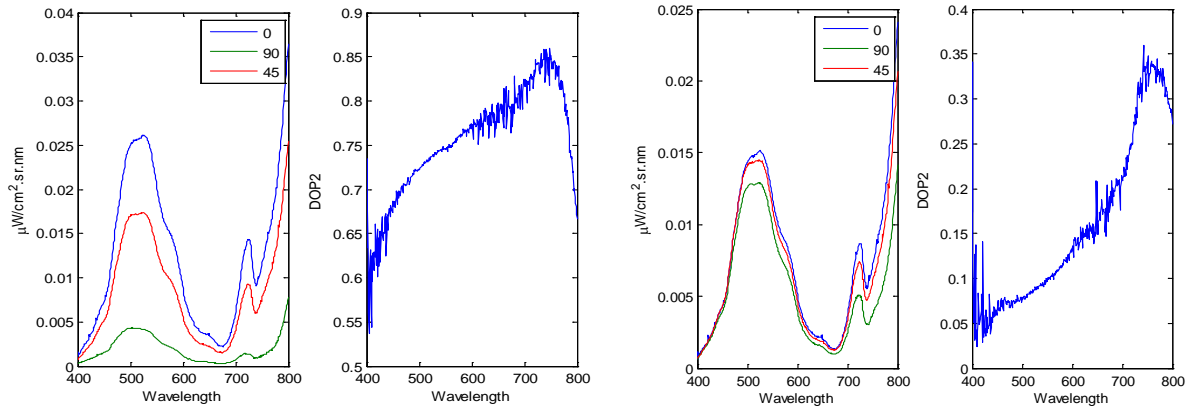
Fig.5 Measured spectra of the light in the fish tank (a,c) and DoLP (b,d) with the polarizer with horizontal orientation in the front in the milk tank (a,b) and in the back (c,d).
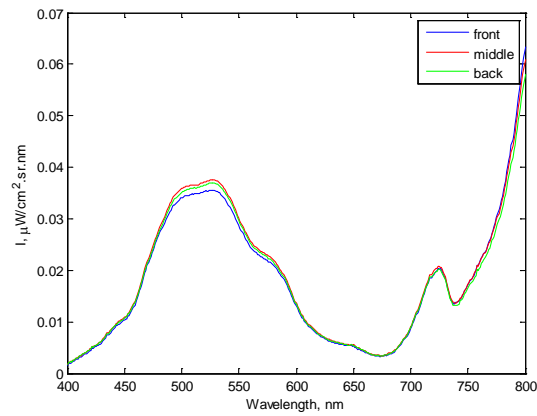
Fig. 6 Spectra of the total radiance I = I0 + I90 for 3 positions of the polarizer in the milk tank (front, middle, back).
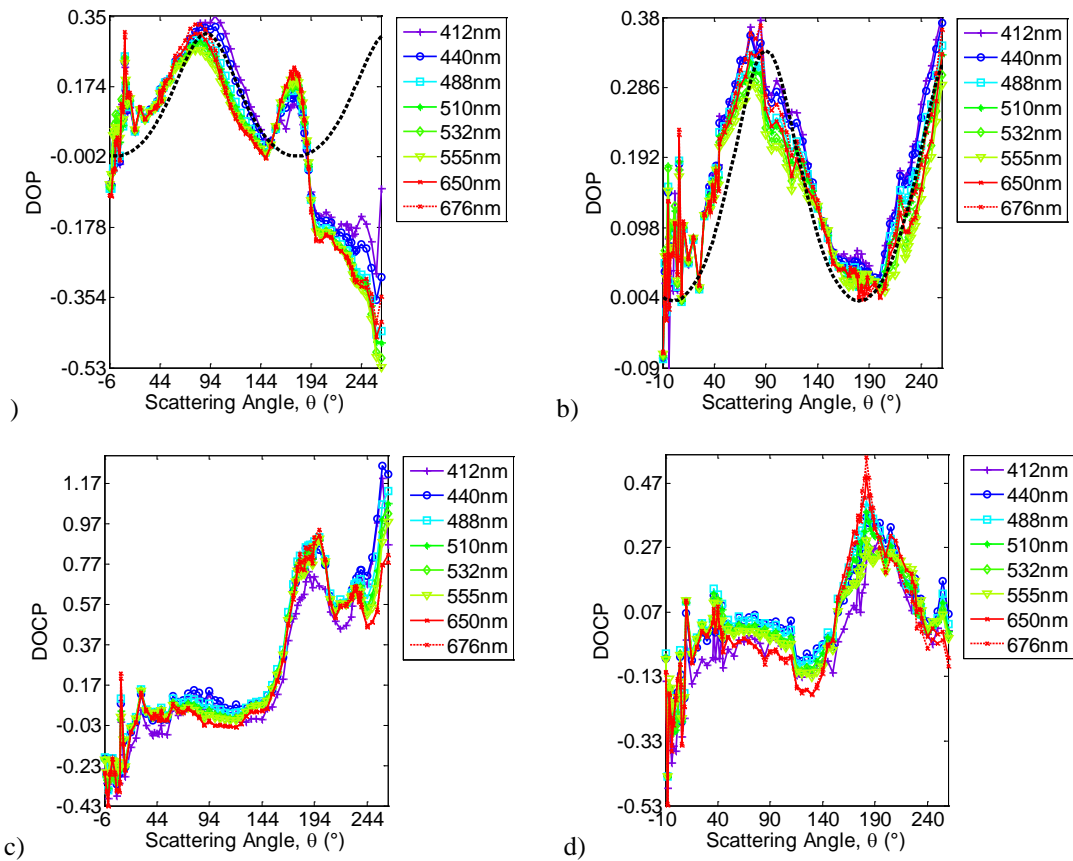
Fig. 7. Shallow water. DoP distributions over scattering angle: a) bottom – sand DoLP, b) bottom – grass DoLP, c) bottom – sand DoCP, d) bottom – grass DoCP
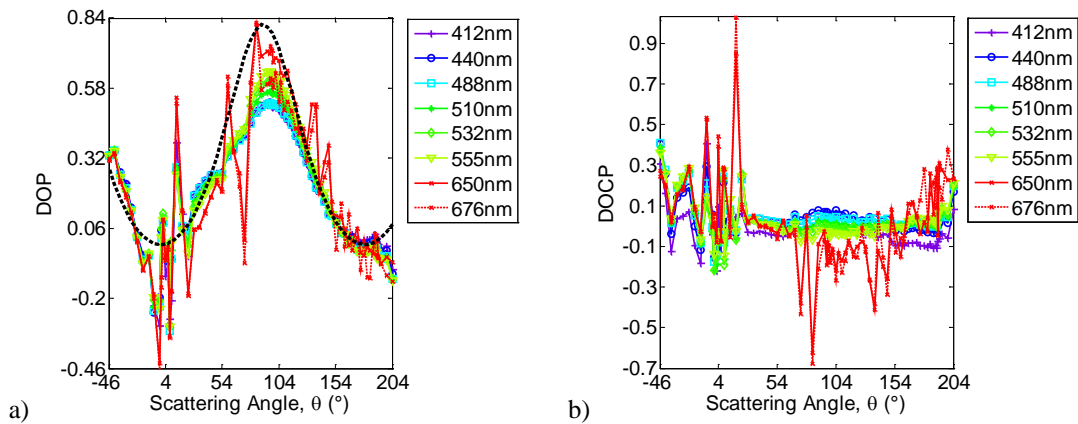
Fig. 8 Open ocean (20 km offshore) DOP distributions over scattering angle measured with the stokes vector radiometer: a) DoLP and b) DoCP.
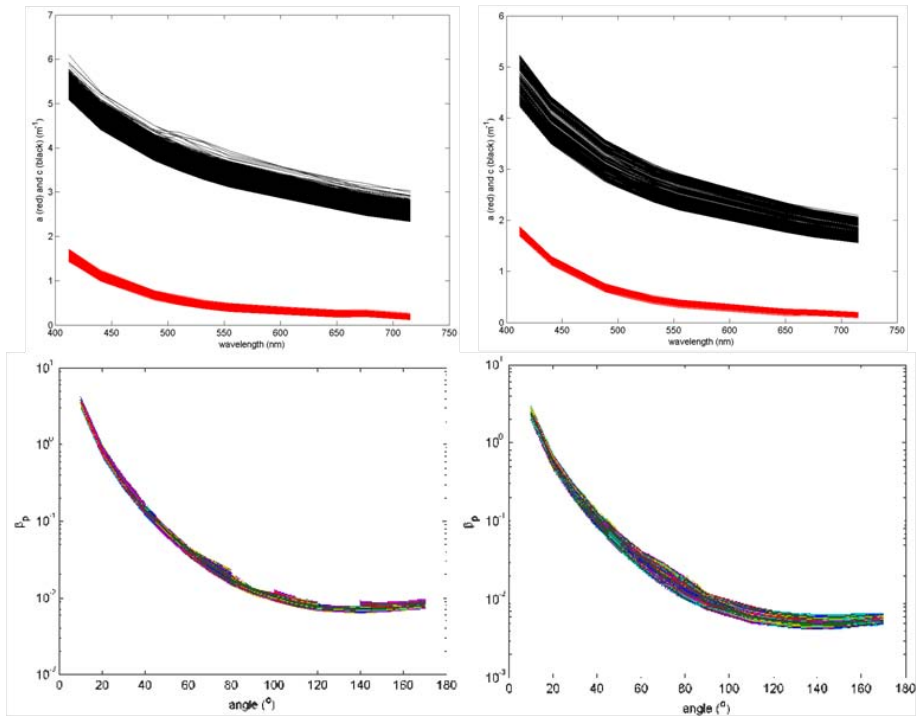
Fig 9. IOP data from eelgrass location 2 (left panels) and 3 (right panels). Absorption (red lines) and attenuation (black lines) for each site are the top panels. The unpolarized particulate VSF are the bottom panels.
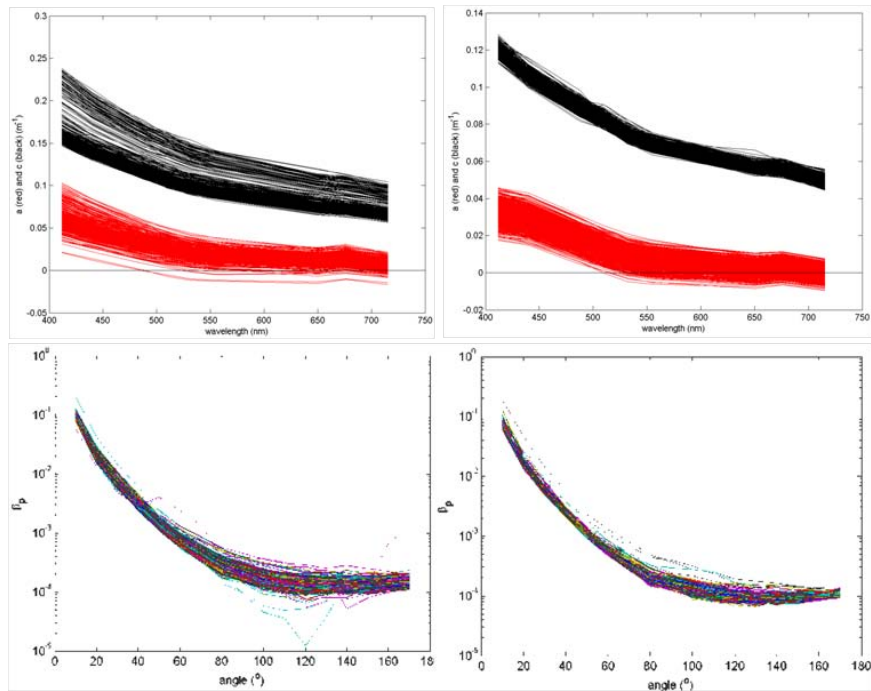
Fig. 10. IOP data from offshsore location 1 (left panels) and 2 (right panels). Absorption (red lines) and attenuation (black lines) for each site are the top panels. The unpolarized particulate VSF are the bottom panels.
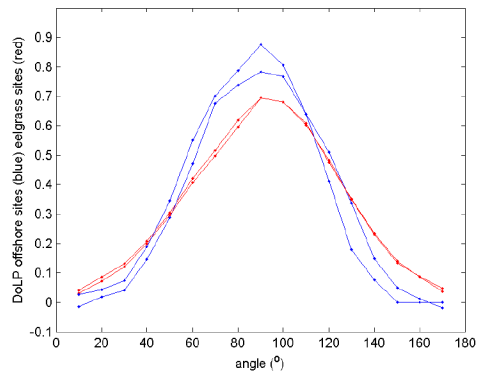
Fig 11. DoLP calculated by using the nts for the two offshore sites (blue lines) and the two eelgrass sites (red lines).
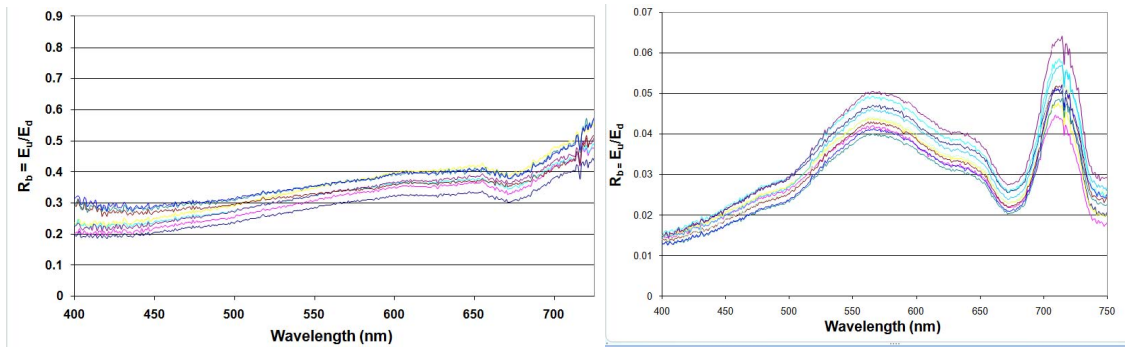
Fig 12.   Benthic reflectance measured 16 June 2010 in Port Aransas Texas over (left) sediment; and (right) seagrass.
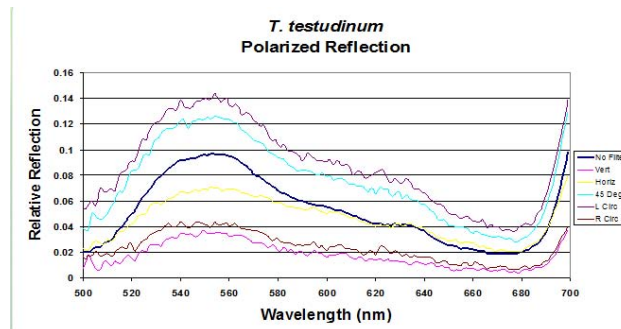
Fig 13.   Laboratory measurements of polarized reflectance over the leaves of the seagrass Thalassia testudinum.
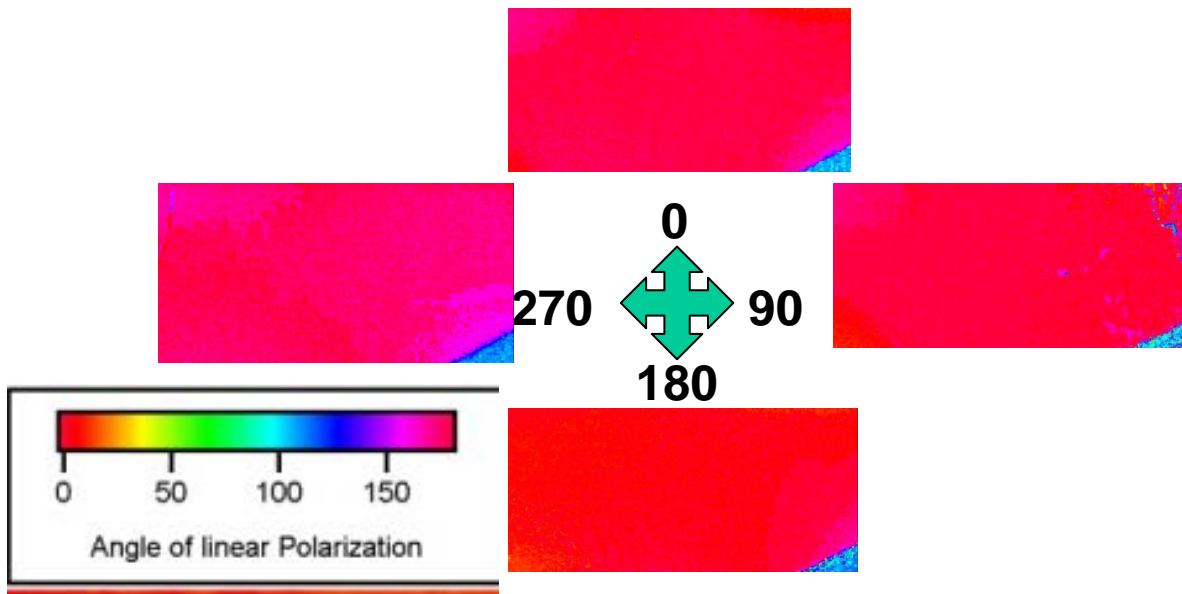
Fig 14. Noon time Seagrass AoLP measurements collected at 0.7m depth in the seagrass beds. Viewing angle (azimuth angle in the horizontal plane) refers to the degrees away from sun direction.
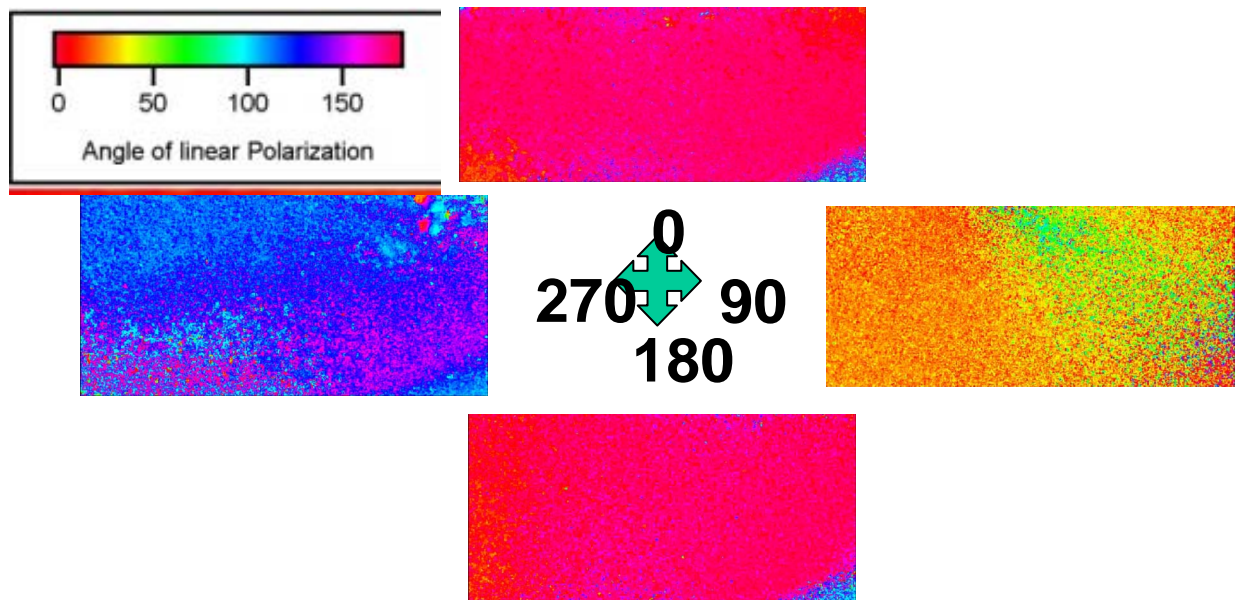
Fig 15. Sunset Seagrass AoLP measurements collected at 0.7m depth in the seagrass beds. Viewing angle (azimuth angle in the horizontal plane) refers to the degrees away from sun direction.
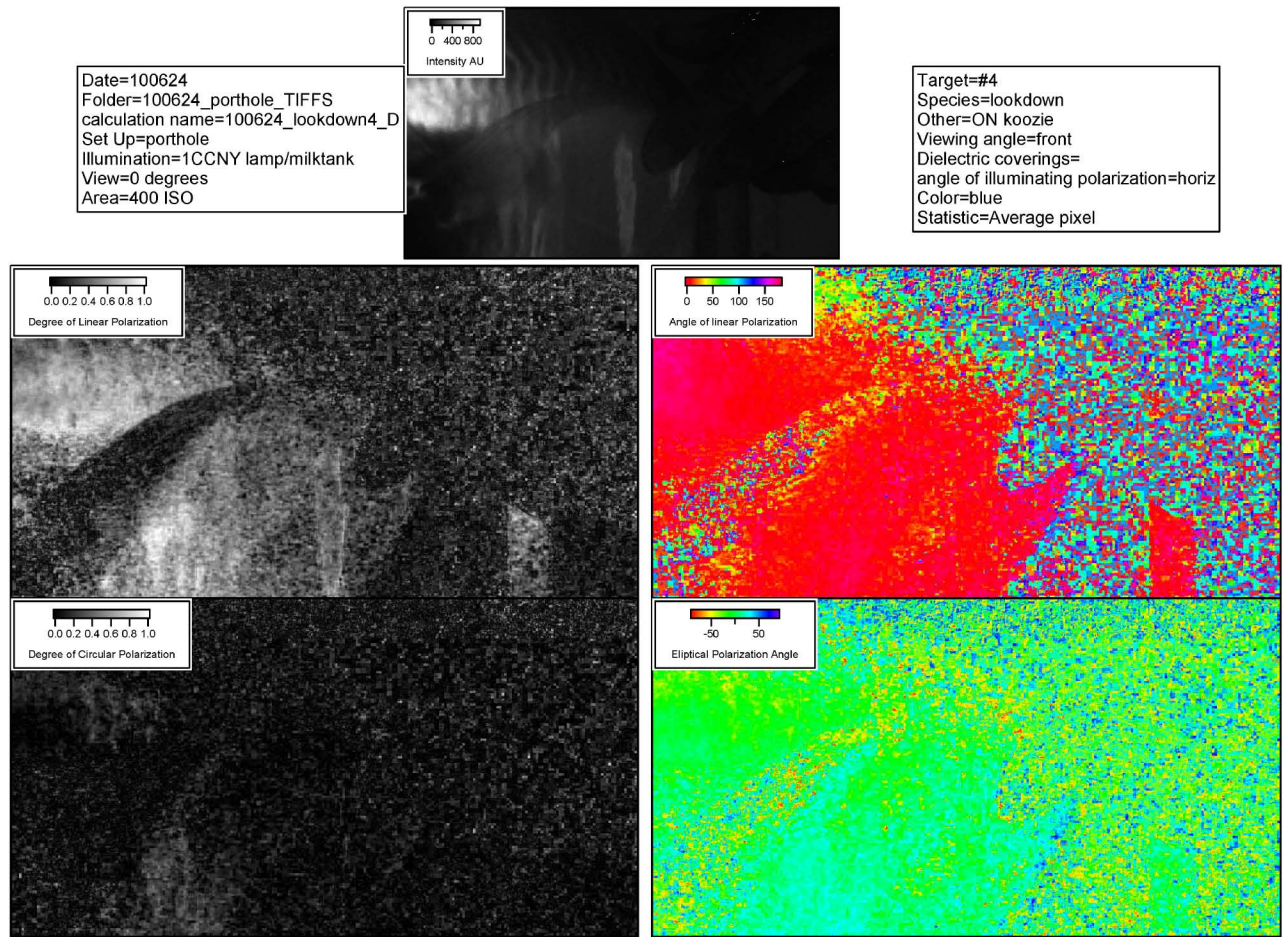
Fig 16. *Underwater videwopolarimeter data from Lookdown (Selene vomer) collected in the experimental tank (Fig 1) at Port Aransas, TX in June.*
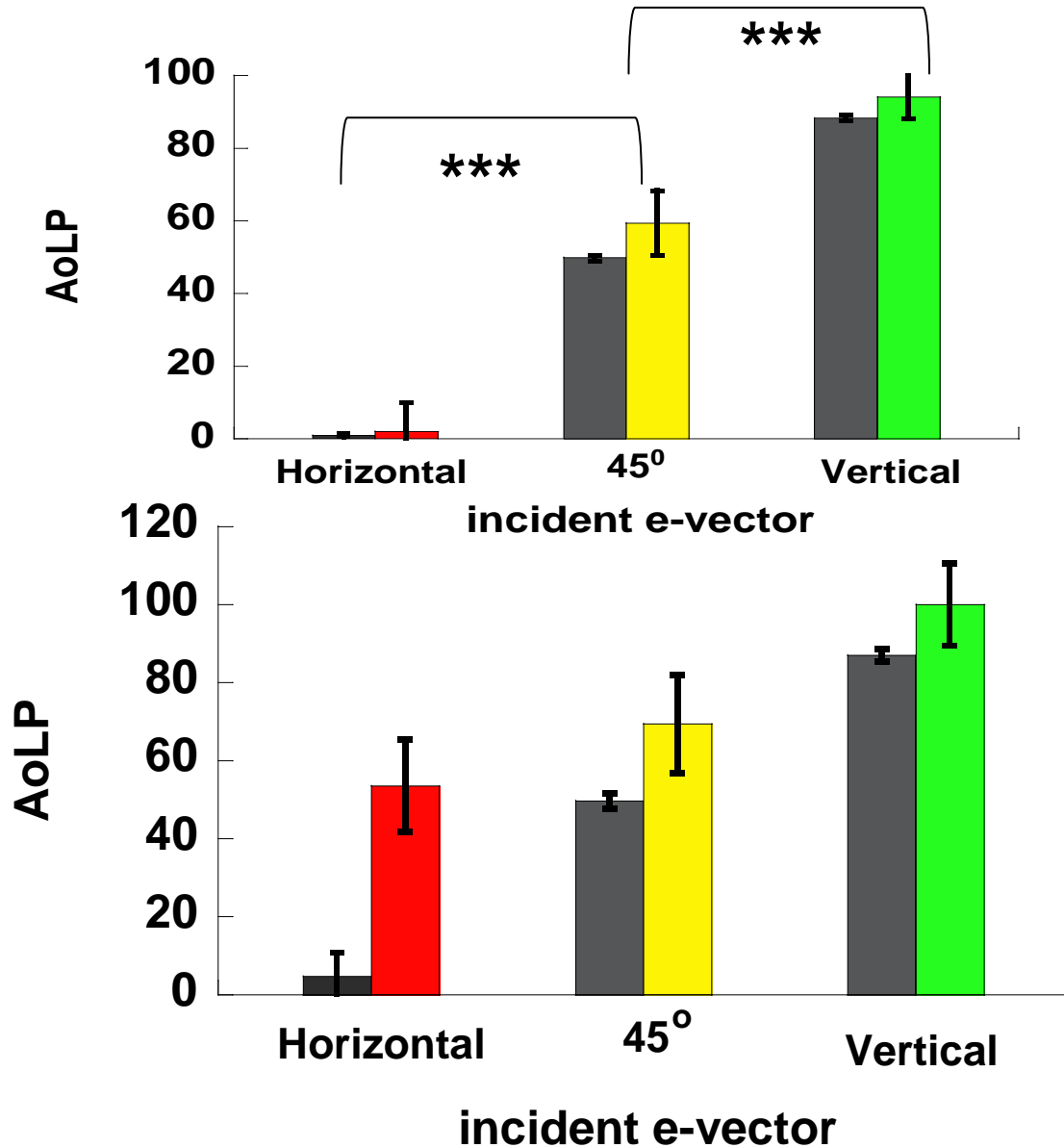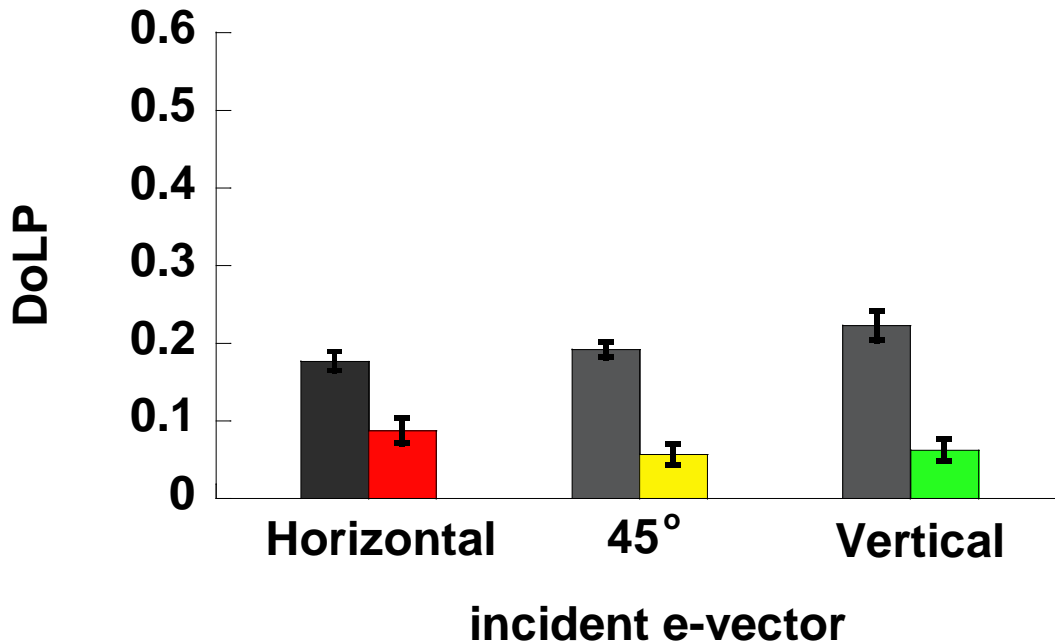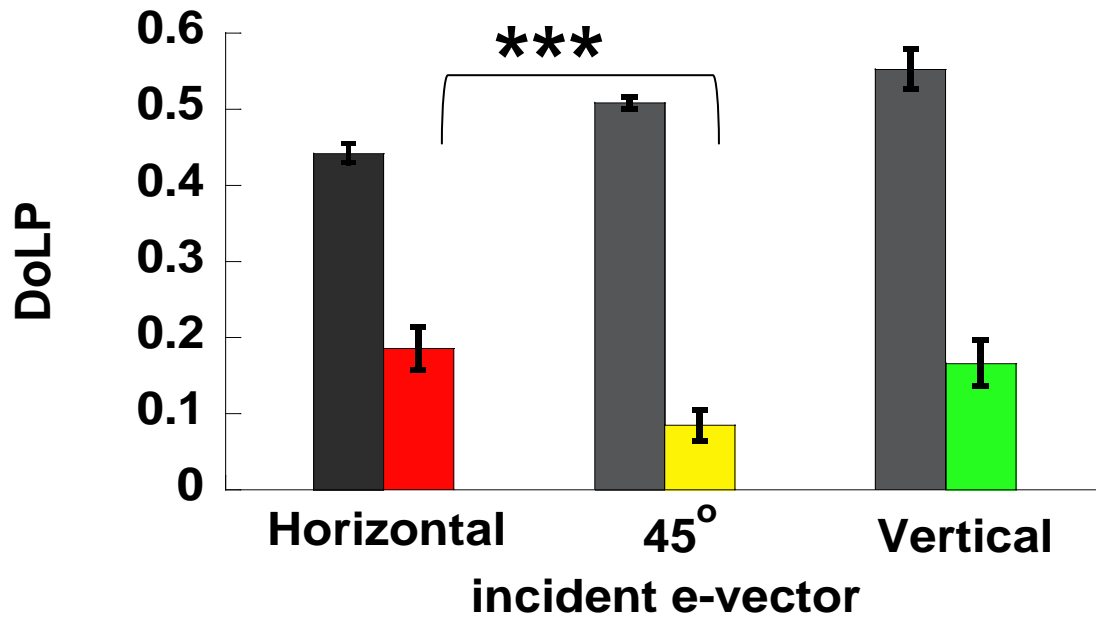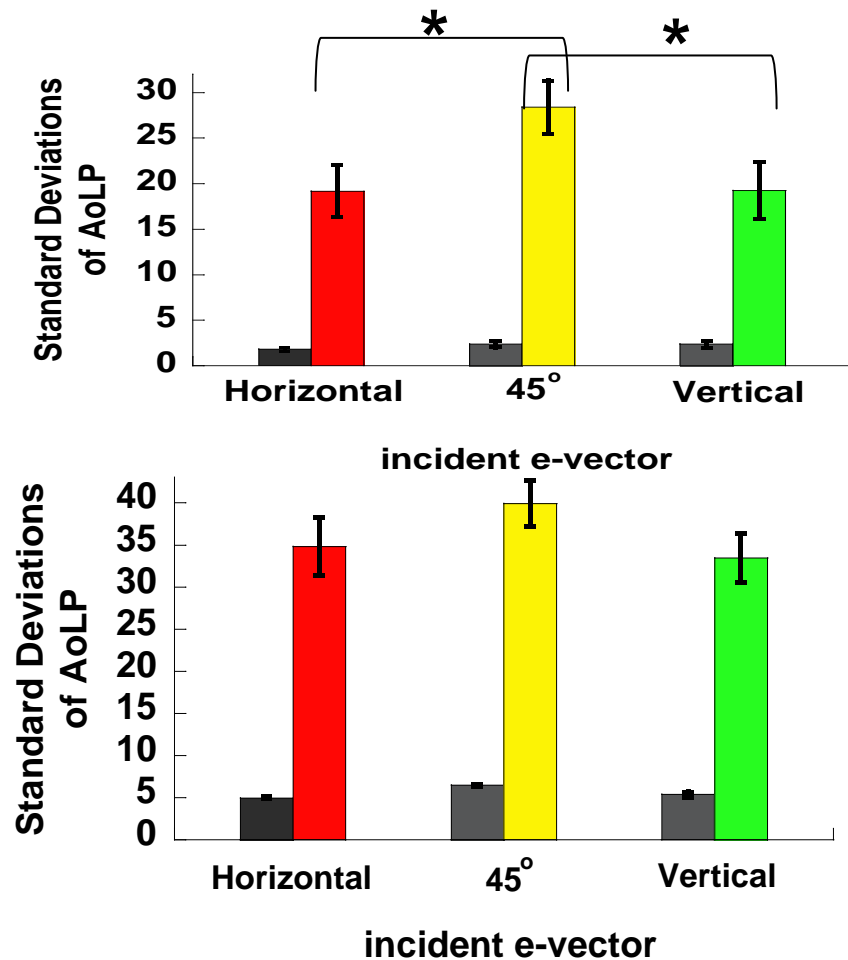
Fig17. Mean AoLP median pixel values from 7 Lookdown midflank regions illuminated in (top) high DoLP conditions (65-80%, see fig 5), and (bottom) low DoLP conditions (5-25%, see fig 5). Colored bars represent lookdown AoLP reflectances illuminated with different incident e-vectors (red= horizontal, yellow = 45°, green = vertical). Grey bars represent the polarization standard reflectance in each condition.
*** represents significance at a p < 0.001 level.

Fig 18. Mean DolP median pixel values from 7 Lookdown midflank regions illuminated in (top) high DoLP conditions (65-80%, see fig 5), and (bottom) low DoLP conditions (5-25%, see fig 5). Colored bars represent lookdown DoLP reflectances illuminated with different incident e-vectors (red= horizontal, yellow = 45•, green = vertical). Grey bars represent the polarization standard reflectance in each condition.
*** * * represents significance at a p < 0.001 level.**

Fig 19. Standard deviations of AoLP measurements from 7 Lookdown midflank regions illuminated in (top) high DoLP conditions (65-80%, see fig 5), and (bottom) low DoLP conditions (5-25%, see fig 5). Colored bars represent lookdown AoLP reflectances illuminated with different incident e-vectors (red= horizontal, yellow = 45°, green = vertical). Grey bars represent the polarization standard reflectance in each condition.
* represents significance at a p < 0.05 level.
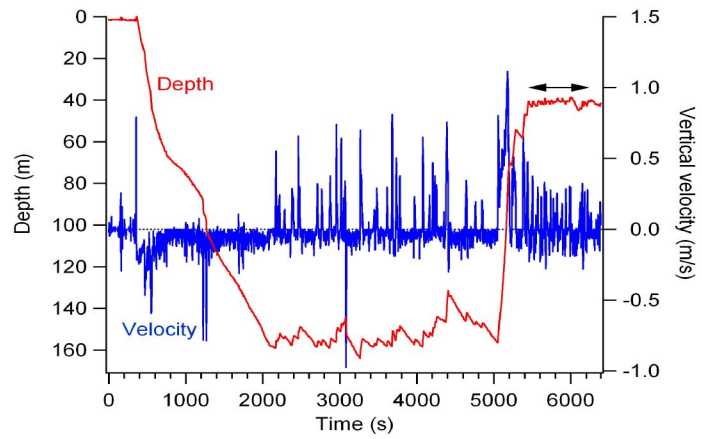
Fig 20. (Left) Releasing a Humboldt squid (Squid 3 in Table 1) fitted with a Crittercam datalogging package from a support vessel next to R/V Horizon. The camera is facing towards the squid's head. (Right) Depth and velocity record of Squid 2 for the entire deployment. The small upwards jets followed by passive sinking at 150 m depth are characteristic 'climb and glide' swimming shown by this species. The time spanned by the arrow at 40 m depth indicates when other squid were present.
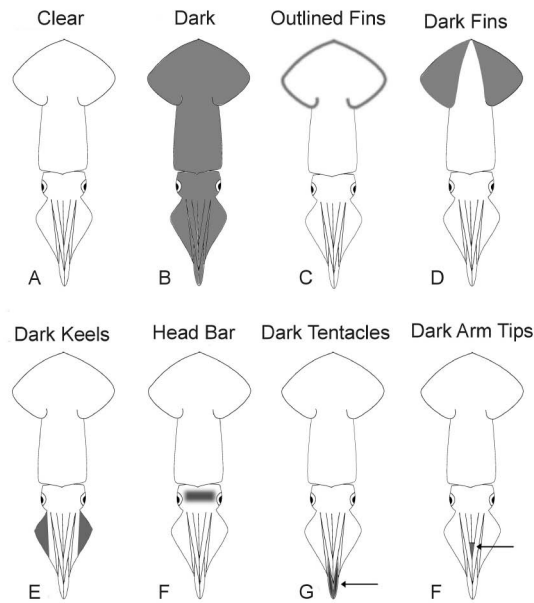

Fig. 21. Chromatic components of Dosidicus gigas observed in squid viewed by the Crittercam under natural lighting. All patterns were maintained for varying amounts of time but the only rapid, repetitive transition was the flashing between Clear and Dark. Patterns E and G) were maintained during rapid flashing over the rest of the body.
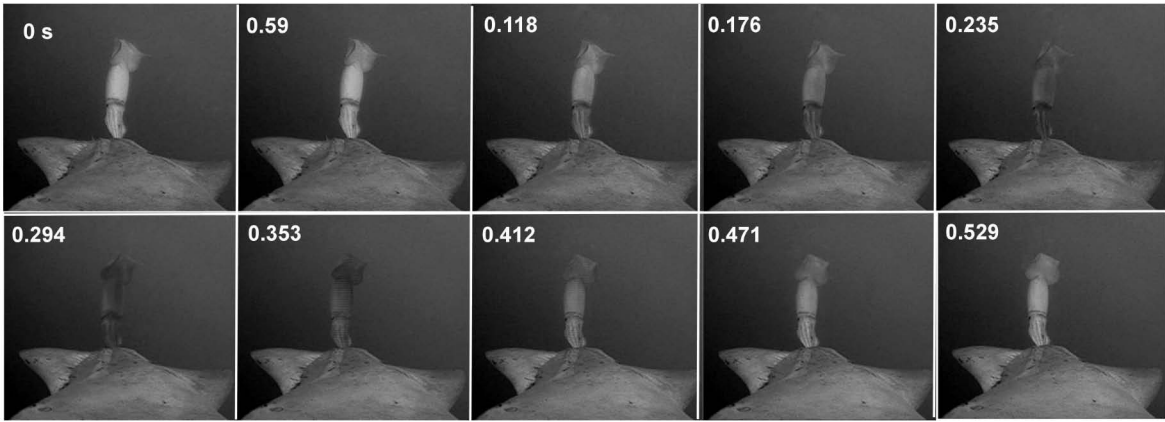
Fig. 22. Whole-body flashing behavior of a viewed squid. Elapsed time is indicated in seconds. This encounter occurred during the interval at 40 m depth noted in Fig. 2. The dorsal surface of the head and arms of the camera –bearing are visible. Flickering occurred during this time interval but is difficult to capture in still images – compare pattern on head in 0.118 s frame with the paler appearance at 0.529 s.
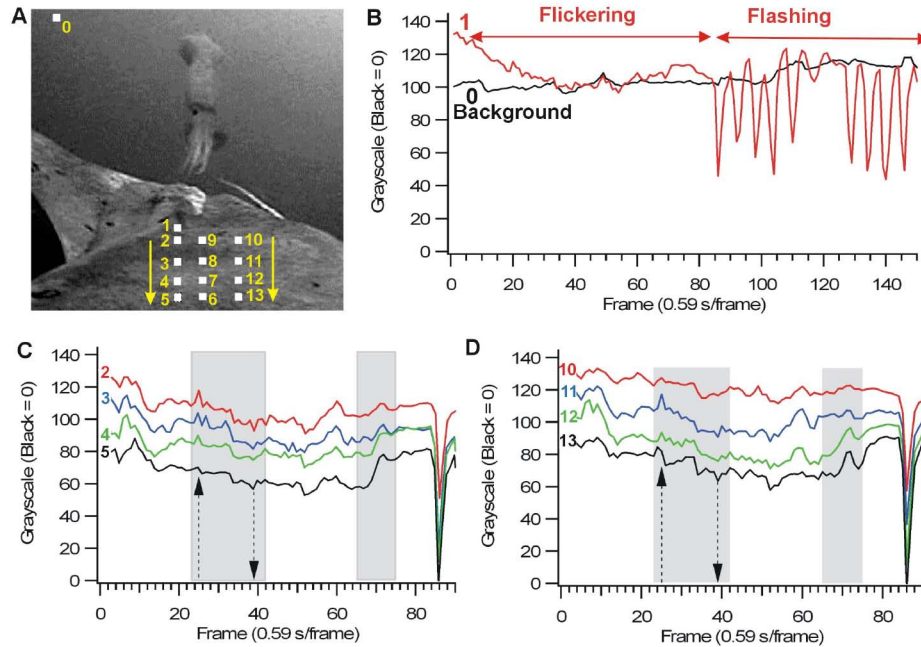
***Fig 23. Flickering behavior of a camera-bearing squid (Squid 3). A.
Time course of grayscale value was analyzed for the numbered white boxes,
including the background (0). B. Typical chromatic activity (box) 1 included
low-amplitude flickering and strong flashing of the entire surface of the head and arms.
C. Chromatic activity in areas 2-3-4-5. The wider gray box highlight synchronous lightening
(up arrow) and darkening (down arrow) at each spot, but relative amplitudes vary from
spot to spot. An decreasing amplitude gradient for the lightening event at frame 25 exists
along the transect from 2 to 5. A decreasing amplitude gradient may exist for the darkening
event at frame 39. Amplitude variability is also evident in the synchronous lightening
highlighted by the narrow gray box. The strong, synchronized darkening at the end of the
record is the onset of the flashing episode. D. Recordings over the same frames for areas
10-11-12-13. The up and down arrows and gray boxes are at the same time points
as in C. Variability is again evident in the relative amplitudes of discrete events from
spot to spot. The vertical scales in C and D only apply to areas 2 and 10, respectively;
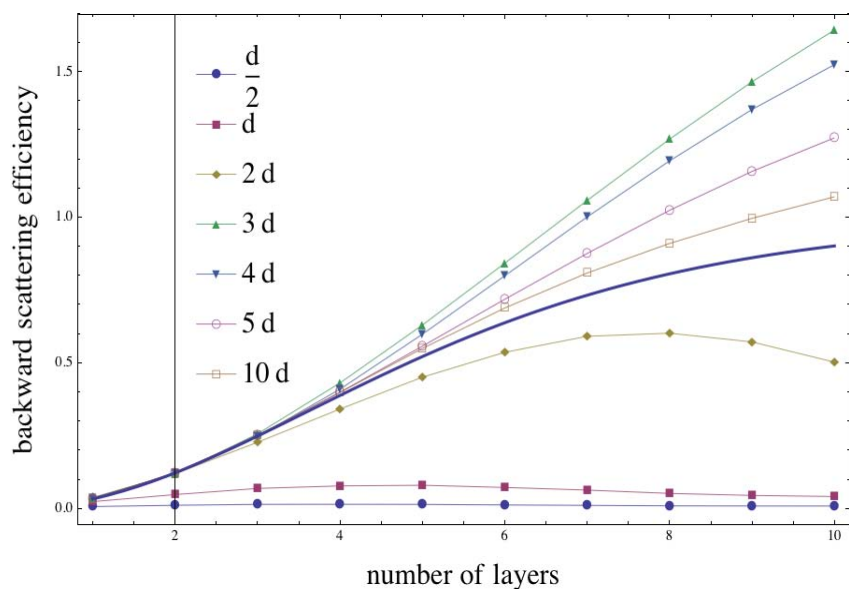the other traces have been shifted vertically to facilitate comparisons.***

22

Fig. 24. Backward scattering efficiency vs. number of layers with different radii. Radii r are shown in the legend, where d=100nm is the thickness of one layer. Incident wavelength is 480nm. The thickness of the spacing between the plates is 120nm. The relative refractive index is $n_r = 1.2$. The thick blue curve is the theoretical result for the semi-infinite plates.
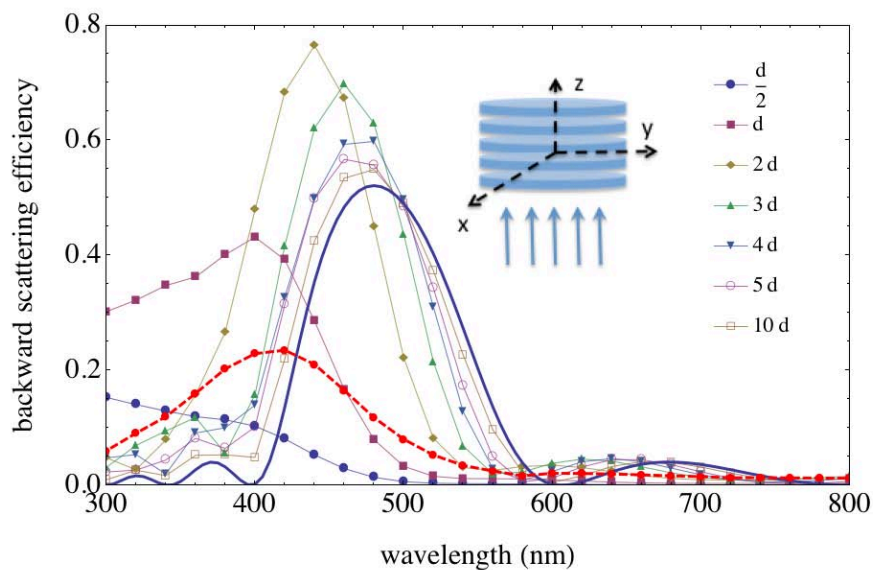

Fig. 25. Backward scattering efficiency of a five layer iridosome vs. incident light at various wavelengths. Radii r are shown in the legend, where d=100nm is the thickness of one layer. The thickness of the spacing between the plates is 120nm. Relative refractive index $n_r=1.2$. The thick blue curve is theoretically calculated for the semi-infinite plates. The red dashed curve is the results of averaged orientations.
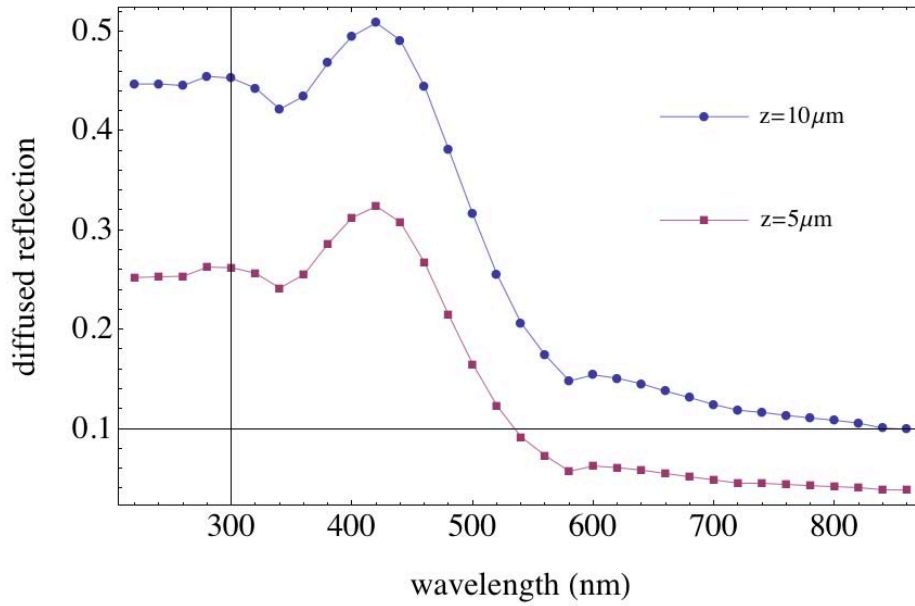
Fig. 26. Diffuse reflection spectrum for a random oriented iridosome layer. The layer thickness is shown in the legend. The thickness of the plate and the spacing between the plates is 100nm and 120nm, respectively. The radius of the plate is 500nm. Incident wavelength is 480nm. Relative refractive index n_r=1.2. The number density of the iridosome is choosen as 1 /μm^3